International Journal of Applied Earth Observation and Geoinformation 122 (2023) 103434

Contents lists available at ScienceDirect

International Journal of Applied Earth Observation and Geoinformation

journal homepage: www.elsevier.com/locate/jag

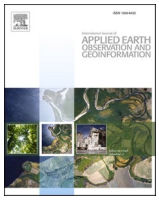

Early-Season forecasting of citrus block-yield using time series remote sensing and machine learning: A case study in Australian orchards

Luz Angelica Suarez *, Andrew Robson, James Brinkhoff

Applied Agricultural Remote Sensing Centre, University of New England, Armidale, NSW 2350, Australia

ARTICLE INFO

Keywords:
Citrus
Yield forecasting
Time series
Remote sensing
Statistical models
Machine learning

ABSTRACT

This study presents a comprehensive evaluation of seasonal, locational, and varietal variations in canopy reflectance responses in 315 commercial citrus blocks from three major growing regions in Australia. The dataset includes three different citrus types (Mandarin, Navel, Valencia) and 26 varieties. The aim is to utilize this combined information to better understand yield variation and develop improved forecasting models. Landsat satellite data spanning from October 2006 to February 2021 (1419 tiles) were used to derive reflectance values, and calculate four vegetation indices (NDVI, GNDVI, LSWI, and GCVI), for each citrus block. These indices were then analyzed alongside corresponding yield data, which consisted of 3660 individual yield records dating back to 2007. Two temporal resolutions were incorporated as predictors: spatio-temporal vegetation index time series (TS) aggregated every two months and annual time series of historical block-yield records. Six statistical and machine learning algorithms were calibrated using a leave-one-year-out cross-validation approach (LOYO CV) and validated for one-year forward prediction over a five-year period (2017–2021). The results highlight significant yield variations across years, alternate bearing patterns, and spatio-temporal changes in reflectance profiles influenced by seasonal conditions, varietal characteristics, and locations. The support vector machine (SVM) algorithm with a radial basis function kernel consistently outperformed other algorithms, indicating a non-linear relationship between citrus yield and predictors. The SVM model achieved an RMSE of 15.5 T ha^{-1}, R^2 of 0.88, MAE of 12.1 T ha^{-1}, and MAPE of 29% in predicting block-yield across farms, varieties, and seasons. These prediction accuracy metrics demonstrate an improvement over current forecasting methods. Notably, the proposed approach utilizes freely available imagery, provides forecasts between two to nine months before harvest, and eliminates the need for infield counting of fruit load for image calibration. This approach provides an improved method for understanding seasonal yield variation and quantifying citrus block-yield, offering valuable insights for growers in harvest logistics, labor allocation, and resource management.

1. Introduction

Accurate pre-harvest yield forecasting is of great importance to growers and the agricultural industry, facilitating informed decision-making regarding market access and forward selling (Zhang et al., 2019). Better predicting total yield as well as its spatial distribution across a farm and over larger spatial extents, can be used to better optimize resources fomenting more responsible and environmental friendly practices (Luo et al., 2022; Zhang et al., 2019). While yield forecasting methodologies have been extensively studied in broad-acre crops like rice, maize and wheat (Basso and Liu, 2019; Schauberger et al., 2020), limited research has focused on tree crops, particularly in the context of block-yield forecasting crops (Brinkhoff and Robson, 2021; Rahman et al., 2018; Schauberger et al., 2020). The unique characteristics of tree crops, including their fixed nature, evergreen leaves, irregular bearing patterns, and extended growth periods, present significant challenges in adapting broad-acre forecasting methodologies to these crops (Ali and Imran, 2021; Sola-Guirado et al., 2017; Zhang et al., 2019).

Tree crops, such as citrus, exhibit flush-based maturity and are subject to alternate bearing, a phenomenon predominantly associated with the source -sink relationship of the tree, that being the translocation of annual accumulated resources such as carbohydrates from photosynthesis to flower and fruit production (Sakai et al., 2008; Somers et al., 2010). A heavy crop load will exhaust the tree's energy reserves and reduce vegetative growth affecting flowering, fruit sites and

* Corresponding author at: University of New England, Armidale, Australia.
E-mail address: lsuarezc@une.edu.au (L.A. Suarez).

https://doi.org/10.1016/j.jag.2023.103434
Received 23 June 2023; Received in revised form 20 July 2023; Accepted 24 July 2023
Available online 30 July 2023

carbohydrate stores for the following season (Bevington et al., 2003). Although this ecological phenomenon occurs at the tree level, yield may become synchronous within larger areas affecting national market prices (Sakai et al., 2008). The alternate bearing process, along with factors like abiotic and biotic stresses, and the complex interplay between yield potential, tree age, and management practices including pruning, contribute to the variability in tree crop yields and introduces a higher level of complexity in yield forecasting (Bevington et al., 2003; Brinkhoff and Robson, 2021; Isagi et al., 1997; Stephenson et al., 1986). Although, some authors, such as Konduri et al. (2020), have indicated weather conditions are the major cause of yield variability in cereals, others have rejected the hypothesis for tree crops, as production at the block level varies to a greater degree than the weather conditions would indicate (Isagi et al., 1997). Stephenson et al. (1986), and more recently Brinkhoff and Robson (2021) found that meteorological variables did not play a significant role in predicting tree crop yield seasonally or across various growing locations.

Existing yield estimation practices in commercial citrus farms involve manual fruit counting, which is labor-intensive and time-consuming (Koirala et al., 2019). This activity is generally undertaken soon after the physiological fruit drop when fruitlets are about 10–15 mm in diameter, typically occurring between 5 and 9 months before harvest. Yield estimations during this period are crucial for improved decision-making regarding budgeting and marketing demand (Dorj et al., 2017). However, recent studies exploring alternative approaches using machine vision and remote sensing techniques have faced limitations in accuracy and practicality, often requiring in-season sampling and struggling with the visibility of fruitlets (Anderson et al., 2021b; Rahman et al., 2018; Robson et al., 2017a).

Yield estimation methodologies using high-resolution satellite (Rahman et al., 2018; Robson et al., 2017a; Robson et al., 2017b) and airborne imagery (Ye et al., 2008; Ye et al., 2007) have been tested with varied results. These studies concluded that the empirical relationships established for each block could not be extrapolated to other locations or seasons due to large yield variability caused by alternate bearing and the variability of the canopy structure resulting from management practices every season. More recent studies have utilized remote sensing and weather data to forecast almond and macadamia block-level yields (Brinkhoff and Robson, 2021; Zhang et al., 2019) at early stages of the growing season, avoiding the need for sampling. However, such research on early block-yield forecasting in citrus crops has been limited, requiring further investigation, especially encompassing a large number of commercial farms and considering the influences of type, variety, location, management, and season.

Although the assessment of sophisticated prediction algorithms in citrus crops has been limited, they offer a wide range of solutions for comprehensive analysis. Leukel et al. (2023) provide a detailed review of machine learning (ML) approaches for predicting grain yield, while Schauberger et al. (2020) present an overview of successful approaches for forecasting yield weeks or months before commercial harvest across various crops. Tree-based algorithms, such as gradient boosting trees, sequentially construct an ensemble of decision trees to rectify errors made by previous trees. Support vector-based algorithms excel in handling high-dimensional data by fitting a regression line while minimizing errors and managing outliers effectively. They can also handle non-linear relationships through kernel functions. Neural network-based algorithms, consisting of interconnected nodes or 'neurons' organized in layers, can model intricate relationships between input and output variables. However, their less interpretable internal workings have led to them being regarded as 'black boxes.' Regression-based algorithms assume a linear relationship between input features and the output variable, decomposing predictors and response variables into a lower-dimensional space defined by latent variables. Detailed information on tuning parameters and internal representation of these algorithms can be found in Kim et al. (2019); Kuhn (2008); and Kuhn and Johnson (2016). All of these algorithms can handle the impact of multicollinearity on model performance through the incorporation of linear and non-linear transformations, along with regularization parameters (Rosipal and Trejo, 2002).

Model assessment is a critical step in evaluating the performance of predictive models, and it involves analyzing several accuracy parameters. However, the choice of specific parameters may vary across different studies, and establishing a standard approach can be challenging (Schauberger et al., 2020). Studies often implement the Root Mean Square Error (RMSE) or the Mean Average Error (MAE) which units are the same as the response variable. MAE, being less sensitive to distant outliers than RMSE, is suitable when the impact resulting from a poor forecast is proportional to the forecast error (Notton and Voyant, 2018; Perez et al., 2013). The Mean Absolute Percentage Error (MAPE, %) is a scale-invariant parameter as it is not affected by the magnitude of the values to be predicted. It treats positive and negative errors equally since it calculates the absolute percentage difference, therefore, the overestimation and underestimation errors have the same impact on the overall MAPE value. MAPE, provides a straightforward interpretation as a percentage error but it is sensitive to zero or near-to-zero values (de Myttenaere et al., 2016; Lee et al., 2022). The Mean Bias Error (MBE) represents the systematic error of a forecast model and indicates whether it overestimates (+), underestimates (−), or shows equal distribution of errors (zero MBE) (Kato, 2016; Mkhabela et al., 2011; Notton and Voyant, 2018). However, MBE is not suitable for evaluating errors of individual predictions. As each parameter possess a particular characteristic and limitation, it is usually recommended the use of different performance metrics to gain a comprehensive understanding of the model's performance.

This study employs a combination of statistical and machine learning (ML) techniques to analyze and forecast block-yield in citrus crops. By comparing several predictive models, our objective is to identify the most effective and consistent method for understanding and predicting future trends and seasonal yield potential across different citrus types, seasons and locations using spatio-temporal data analysis of Earth observation data and historical production. Our aim is to surpass current commercial practices and eliminate the need for in-season sampling. The study encompasses three major citrus-growing regions in Australia to ensure robustness and scalability to other locations.

In addition to forecasting future yields, our study compiles a comprehensive dataset directly provided by growers, covering over a decade of block-level information from multiple locations. This dataset enables the description of reflectance profiles based on phenological stages, age, location, and citrus type, shedding light on patterns and potential effects on forecast performance, robustness, and scalability. We also explore different temporal resolutions of time series data, Earth observation data, and historical production as predictors to determine the optimal combination for accurate forecasting. Moreover, we assess the selected model's ability to predict production trends.

By addressing these research objectives, our study aims to bridge the existing gap in citrus early block-yield forecasting and contribute to the advancement of model selection and decision-making processes in the citrus industry.

2. Materials and methods

2.1. Study area

Three main growing regions in Australia were incorporated in this study: Riverland, Sunraysia (Murray Valley) and the Wheatbelt (Western Australia) (see Fig. 1). About 44% of Australia's citrus production occurs in these regions. For all the regions, the main crop is Navel, followed by Mandarin and Valencia. Navels represent 65% of planted area in Sunraysia, 51% in the Riverland and 49% in the Wheatbelt region and Mandarin (Valencia) represents 23% (6%), 25% (17%) and 28% (15%), respectively. Of the total citrus planted area, this study analyzed 27% of the Wheatbelt region, 14% of the Riverland and 3% of Sunraysia. The

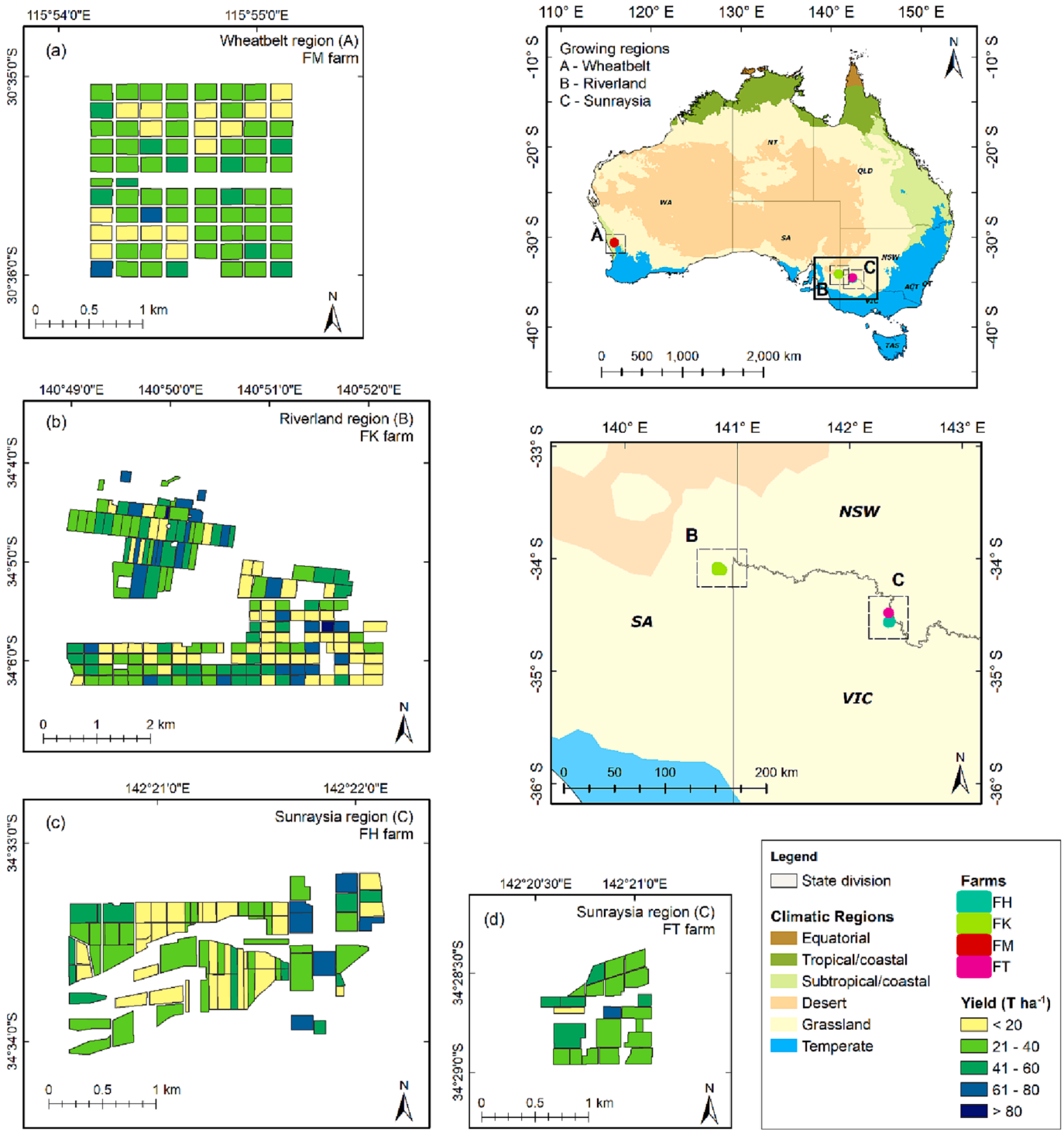

Fig. 1. Long-term mean yield of citrus blocks located the main growing regions in Australia. Location of (a) KM farm, (b) FK farm, (c) FH farm and (d) FT farm. Climatic classification map sourced from Bureau of Meteorology (2023).

most common varieties (national planted area) were included such as Leng (2%), M7 (2%), Navelina (3%), Washington (10%), Late Lane (10%), Cara Cara (3%), Valencia (16%), Imperial (5%), Afourer (8%) and Murcott (4%) as well as 16 lesser produced varieties (Table S1). Farms of different sizes (named as FH, FK, FM, and FT) with citrus blocks of various age (maturity), varieties, management practices and historical production were included in this study (Fig. 1). Management practices, including row spacing, irrigation scheduling, pruning, fertilization, and soil management, varied across blocks to meet market demands and farm production calendars. Crops under permanent netting were excluded from the analysis due to the non– canopy related influence they have on the EO data. Citrus blocks were distributed across two climatic regions (Bureau of Meteorology, 2023): grassland (GL) and subtropical (SBT). More specifically, the grassland blocks were located in the Riverland (FK) and Sunraysia growing region (FH, FT) and the subtropical blocks (FM) were located in the Wheatbelt growing region.

Meteorological data from the SILO database (2007–2021) was collected for each farm, including rainfall and temperature records. R software was used for further analysis. Long-term mean values of annual and monthly rainfall and temperature were calculated by climatic region

(Fig. S1). The GL-blocks had a mean maximum temperature of 24.9 °C, while SBT-blocks experienced temperatures approximately 2 °C higher. GL blocks had a mean monthly rainfall of 45.6 mm, and SBT blocks had 32.1 mm. Rainfall in the GL region declined rapidly since 2016 but showed a slight increase in 2020. In 2019, both regions experienced their lowest recorded rainfall due to severe drought. Despite the drought, all blocks analyzed were irrigated, minimizing immediate production impacts. The diverse growing conditions, encompassing crop type, age, management practices, and climate variations, allowed for scalability and robustness of the study.

2.1.1. Growing cycle of citrus

In Australia, most of the citrus blocks are harvested by October. However, in very few cases, depending on the variety harvest can be extended until November. Between October and November flowering and fruit set occur accompanied by the first flush of new shoot growth. From here, fruit growth, particularly cell division occurs until December, followed by cell expansion until April and maturity until harvest (June – September) (Table 1) (Bevington et al., 2003). Commercially, three yield estimates during the growing season take place: a) during latest phase of flowering and Stage I of fruit growth, b) after a physiological drop usually at the beginning of the Stage II of fruit growth, and c) during the latest stages of maturation just before harvesting. Decisions around crop intervention occur during the second yield estimation when crop load is set, therefore the timing of this estimate is the most important one for farm operations, and it is the focus of this study.

2.2. Data

2.2.1. Historic yield records

Block-yield records (in tons per hectare, T/ha) and farm maps detailing block boundaries, varieties and planting year and area (ha) were provided by the participating growers. Initially, 3660 individual yield records extending back to 2007 were collated. The dataset contained information on management practices, planting year per block (from 1966 to 2018, average tree age = 15), production (0.1 T ha^{-1} – 122 T ha^{-1}), harvest seasons (2007–2021), block area (0.5 ha – 14.6 ha) and location (4 farms). Each individual block had uniform tree age, management, irrigation scheduling and variety. From the data, block level yield varied greatly between citrus types and years (Fig. 2). Mandarin blocks displayed the greatest variation in yield within and across seasons (spatial and temporal variability), whereas Navels had less spatio-temporal variability. Valencia yields showed greater temporal variability, but yields were similar across blocks within a season. The average yield of Mandarin blocks was 37.7 T ha^{-1} (standard deviation, SD = 22.9 T ha^{-1}), 35.1 T ha^{-1} for Navels (SD = 15.5 T ha^{-1}) and 40.5 T ha^{-1} for Valencia (SD = 18.6 T ha^{-1}).

For each record (block per season), the historical block-yields of the previous three years were added to the dataset generating the time series (TS) of historical yields (TS-HY), hence only blocks with such historical information available were used. This accumulation of data supports a better understanding of alternate bearing of the citrus crops. Therefore, the TS-HY dataset started in 2010 and included data of the previous three years (2007, 2008 and 2009). Blocks with "no data" or 0 T ha^{-1} records were removed for calibration purposes, reducing the number of valid records to 2382.

2.2.2. Block boundaries and spatio-temporal satellite data

All block boundaries were digitized using ArcGIS as shapefiles and imported into Google Earth Engine (GEE) (Gorelick et al., 2017) to extract spatio-temporal information at the block level. Landsat 5 TM, 7 ETM+, and 8 OLI surface reflectance data (collection 2, tier 1) from October 2006 to February 2021 was accessed. Landsat imagery was selected for its adequate spatial and temporal resolution. The data were processed in Google Earth Engine (GEE) at a 30-meter spatial resolution. Although harmonizing the reflectance data from different sensors is often considered important, previous research by Brinkhoff and Robson (2021) indicated that harmonization did not lead to improved model performance. Furthermore, a random assessment of time series at the block level did not reveal significant changes in the profile. Therefore, the step of harmonizing the data from different sensors was omitted in this study. To account for cloud cover, the USGS CFMASK cloud mask was applied to all imagery prior any calculations. A total of 1419 tiles were processed and four vegetation indices (NDVI, GNDVI, LSWI, and GCVI) were calculated per tile to describe yield variability without introducing excessive variables or overfitting (Table 2) during the modeling stage. To address mixed pixel issues, the spatial mean per block (per tile) was calculated, giving more weight to homogenous pixels enclosed within block boundaries. A minimum (maximum) of 324 (575) tiles were available per block (average = 387). Fig. S2 shows the distribution of tiles per capture year and month. The resulting remote sensing (RS) dataset was then imported into R software (R Core Team, 2014) for further analysis.

To enhance data availability and mitigate the impact of cloud cover, RS data was aggregated into a two-month period (bTS) per block. This approach increases the likelihood of having data for analysis and modeling by reducing the obstruction caused by cloud cover. Moreover, aggregating the data over a bimonthly timeframe provides a more comprehensive understanding of the block's characteristics and trends. It helps minimize the influence of outliers or noise present in individual pixels while creating a smoothing effect on the data. As such, six periods (P) were defined encapsulating key developmental stages. The first period (1P) started in October (~after harvest) and 6P ended the following September (Table 1). Similar approaches of aggregation according to phenological-related stages have been reported by Brinkhoff

Table 1
Key growth stages of citrus blocks during calendar year and periods of analysis. Letters (a, b, c) indicate (usual) timing of the three commercial estimates performed in Australia.

Month of the year	Jan	Feb	Mar	Apr	May	Jun	Jul	Aug	Sep	Oct	Nov	Dec
Period (P)	2	3		4		5		6		1		2
Key growth stage												
Floral induction and initiation												
Pre-bloom												
Flowering										a		
Stage I Fruit Growth											a	
Stage II Fruit Growth	b	b										
Maturation/Harvest					c	c	c					

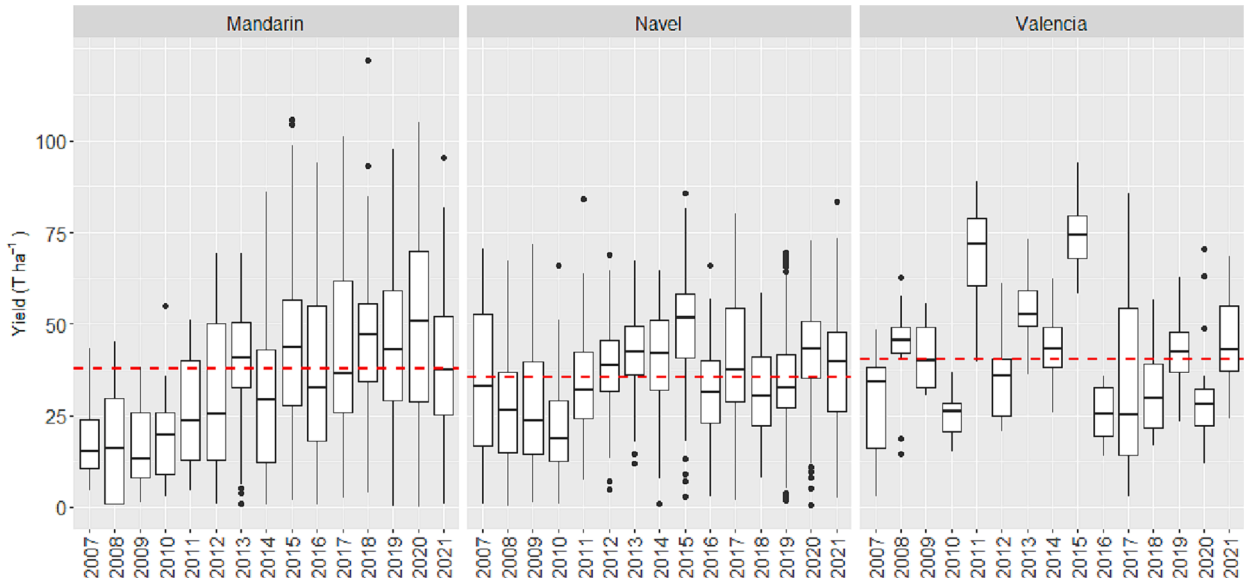

Fig. 2. Historical production by citrus type. The dotted line represents the average yield across the seasons per citrus type.

Table 2
Summary of vegetation indices used in the block-yield forecast.

Vegetation Index (Abbreviation)	Equation*	Reference
Greenness normalized difference vegetation index (GNDVI)	(NIR-Green)/(NIR + Green)	Gitelson (2011)
Normalized difference vegetation index (NDVI)	(NIR-Red)/(NIR + Red)	Tucker (1979)
Land Surface Water Index (LSWI)	(NIR-SWIR1)/(NIR + SWIR1)	Chandrasekar et al. (2010)
Green Chlorophyll Vegetation Index (GCVI)	(NIR/Green)-1	Gitelson et al. (2003)

* *Abbreviation in the equations:* NIR, Near infrared; SWIR1: Short wave infrared

and Robson (2021) and Gomez et al. (2019). The bTS of the previous three years were also added creating the final TS-RS.

The TS-RS and the TS-HY datasets were merged creating the level 1 (L1) dataset that included all three citrus types and all potential predictors (detailed in 2.3.1). Thus, each record (block per season) incorporated two TS of different temporal resolution: bimonthly (TS-RS) and annual (TS-HY), each of them with the respective three years of historical information. For modeling, each record had a complete set of observations (i.e. no missing values).

2.3. Methods

The following sections describe the main approaches implemented in this study and are illustrated in Fig. 3.

2.3.1. Selection of the best predictors

The performance of models can vary based on the set of predictors used. This is because different algorithms have varying capacities to transform non-linear relationships between predictors and the response variable, as well as to minimize overfitting to noise in the training data. Models can extract features from different parts of the dataset that best describe the response variable. Therefore, the selection of predictors prior to model calibration can impact the results. In order to determine the best set of predictors, models were calibrated and validated using each set, and the set that consistently demonstrated the highest performance according to the RMSE (Eq. (1)), the MAE (Eq. (2)), and MAPE (Eq. (3)) was selected. Six sets of predictors were tested (Table 3). These included combinations of:

a) historical yields of the previous 3 years (3HY);
b) historical RS data defined by the four VIs for each period of the previous 3 (3ys) or two (2ys) years; and
c) current RS data of the four VIs during the first and second growth period of the current harvest season (1P and 2P respectively).

We further explored the relationships between individual predictors and block-yield (Table S2 and Fig. S3) to gain insight of such relationships and their relevance on model performance.

2.3.2. Modelling approach

We employed a combination of statistical and machine learning (ML) techniques to analyze and forecast yield in citrus crops. Each of these algorithms utilizes distinct decomposing approaches to learn the relationships between the response and predictor variables, with specific tuning parameters controlling their behavior and influencing how they learn from training data and make predictions. Further information can be found in Kuhn and Johnson (2016). Table 4 lists the tuning parameters for each regression algorithm.

For model calibration purposes, Leave-One-Year-Out Cross-Validation (LOYO CV) was implemented. In this approach, the training dataset was split by season, ensuring that data from each year was used for validation while the remaining years were used for training. The performance of the model, as measured by RMSE, was assessed by systematically varying the tuning parameters. The optimal tuning parameters were determined by selecting the set of values that yielded the smallest average RMSE across the LOYO CV process. Once the optimal tuning parameters were identified, the entire training dataset was used to train the final model, employing these selected parameter values.

The final models underwent independent validation using a one-year forward season (test dataset, t). This validation process was repeated five times for each year from 2017 to 2021 (t_{2017}^{2021}). This approach was chosen to replicate real-world conditions, where forecasting block-yield for a new season relies solely on the previous season's data.

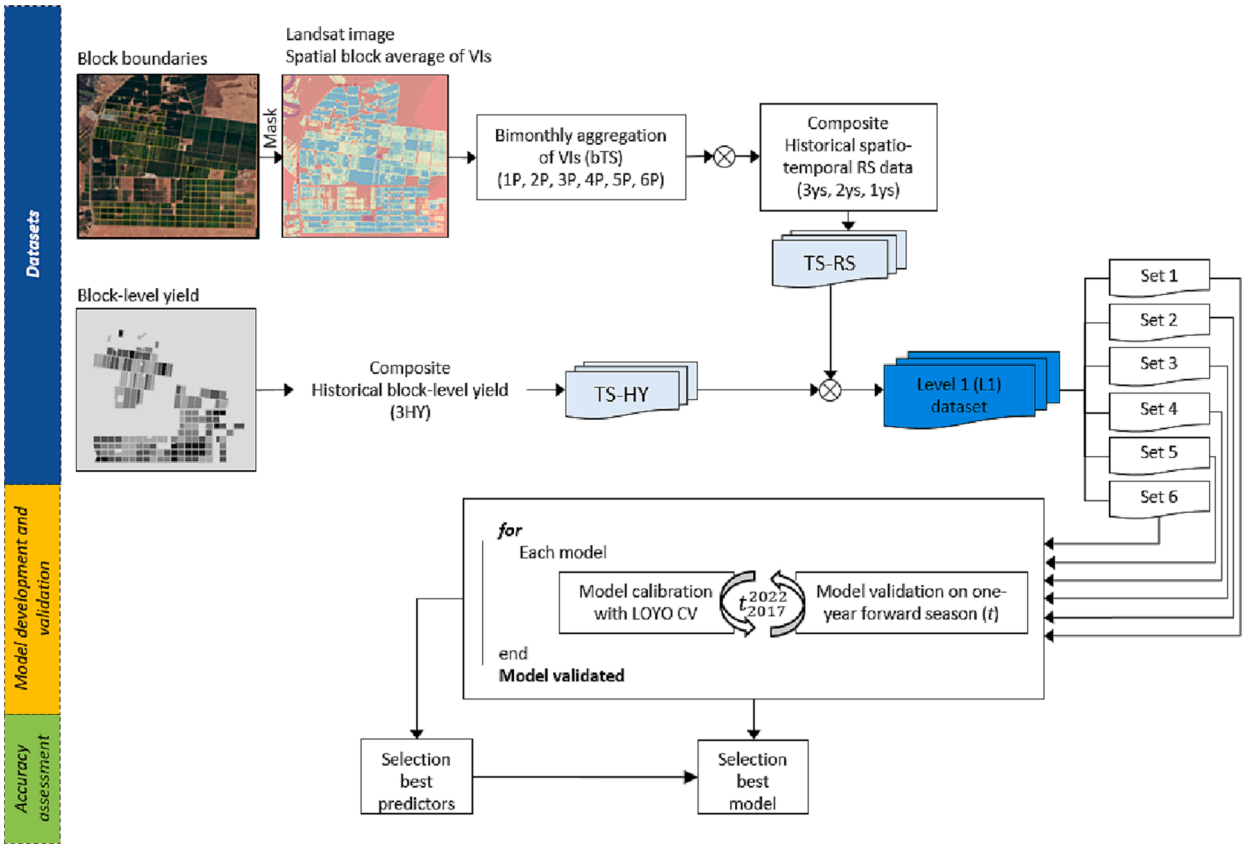

Fig. 3. Illustration of dataset compilation and modeling approach for citrus block-yield forecasting.

Table 3
Group of predictors, predictor origin and total number of predictors for modeling purposes. 3HY: Historical yields of the previous 3 years; 2ys (3ys): historical RS data defined by the four VIs for each period of the previous 2 (3) years; 1P (2P): RS data as per the four VIs during the first (second) period of the current harvest season.

Set	Predictors	Abbreviation	Origin of predictors	Number of predictors
1	3HY	yield	TS-HY	3
2	2ys + 1P + 2P	2ys + p1 + p2	TS-RS	56
3	3ys + 1P + 2P	3ys + p1 + p2	TS-RS	80
4	2ys + 1P + 2P + 3HY	[2ys + p1 + p2] + yield	TS-RS & TS-HY	59
5	3ys + 1P + 3HY	[3ys + p1] + yield	TS-RS & TS-HY	79
6	3ys + 1P + 2P + 3HY	[3ys + p1 + p2] + yield	TS-RS & TS-HY	83

Additionally, it allowed us to gain insights into the temporal stability of the models.

2.3.3. Model assessment

Accuracy prediction parameters, including RMSE, MAE, MAPE, and MBE (Eq. (4), were calculated to assess the performance of the models. A temporal analysis of the accuracy parameters was further conducted to identify the most stable and reliable model among the validation seasons.

$$RMSE\left(Tha^{-1}\right) = \sqrt{\frac{\sum_{i=1}^{N}(\hat{y}_i - y_i)^2}{N}} \quad (1)$$

$$MAE\left(Tha^{-1}\right) = \frac{1}{N} \times \sum_{i=1}^{N} |\hat{y}_i - y_i| \quad (2)$$

$$MAPE\,(\%) = (MAE/\overline{Y})*100 \quad (3)$$

$$MBE\left(Tha^{-1}\right) = \frac{1}{N} \times \sum_{i=1}^{N} (\hat{y}_i - y_i) \quad (4)$$

where N is total number of block-yields i, $\hat{y}$ and y refer to the predicted value and the actual value and $\overline{Y}$ refers to the mean of actual values.

To gain insights into how these models make predictions and aid in further model selection, the calculation of variable importance (VImp) scores was employed. The models present varied challenges in interpretation. Certain models, such as partial least squares, gradient boosting, and neural networks, inherently quantify the influence of predictors in different ways (Scholbeck et al., 2020). However, some algorithms, like support vector machines, lack this capability, limiting our understanding of their predictions. To address this, a standardized model-specific method was implemented to compute VImp scores (Greenwell et al., 2018), which can be utilized with any trained supervised algorithm. In this approach, the most important variable for each model is assigned a score of 100%, while subsequent variables receive relative values between 0 and 100, indicating their proximity in importance to the first variable. It is important to note that the VImp scores are relative and serve as indicators of the absolute value of the effect, rather than the sign or direction.

Subsequently, the chosen model was utilized to estimate the total production for each citrus type at the farm level, aiming to evaluate its capability in predicting production trends.

Table 4
Algorithm and tuning parameters used in this study.

Model	Tuning parameter(s)	Abbreviation
Partial Least Squared Regression	Number of components	plsr
Bayesian Regularized Neural Networks	Number of neurons	brnn
L2 Regularized Support Vector Machine (dual) with Linear Kernel	Cost (c) and Loss (loss) Function	svmLinear3
Support Vector Machines with Radial Basis Function Kernel	Sigma and Cost	svmRadial
eXtreme Gradient Boosting	Number of boosting iterations, L2 regularization (lambda), L1 regularization (alpha), and the learning rate (eta)	xgbLinear
Neural Networks with Feature Selection (Principal Component Step)	Size (Hidden Units) and decay (Weight Decay)	pcaNNet

2.4. Results

2.4.1. Citrus phenology and reflectance profiles

The reflectance values of Mandarin, Navel, and Valencia blocks were aggregated into two-month periods representing different growth stages (Table 1 and Fig. 4). During flowering (~1P), the visible (VIS) reflectance reached its highest values due to a higher number of immature leaves in the canopy and their biochemical and biophysical composition with the lowest chlorophyll content and therefore a low photosynthetic capacity limiting the energy absorption in this region (Mustafa et al., 2005; Stuckens et al., 2011). From Stage I (fruit setting, 1P-2P) to Stage II (~3P-4P), the reflectance declined consistently as the citrus leaves matured, resulting in increased energy absorption in the VIS region due to higher chlorophyll content (Mustafa et al., 2005). The reflectance decreases between 3P and 4P are associated with root and shoot growth flushes and fruit development (cell expansion) (Bevington et al., 2003; Iglesias et al., 2007). At the maturation stage (5P), the reflectance values reached their lowest point, corresponding to a fully developed canopy with maximum radiance absorption, driven by high chlorophyll content and larger leaf area (Somers et al., 2010). After maturation, the trees entered the senescence or dormancy stage (6P), leading to a slight increase in reflectance values associated with a decrease in chlorophyll content (Mustafa et al., 2005). Variations in the reflectance curve at the farm and block level reflect different management strategies, locations, health, and tree age (Fig. 4). The GNDVI values increase as trees mature, with the highest values observed in trees around 15 years old. Younger trees have lower GNDVI values due to smaller canopies and more soil exposure, while trees between 10 and 15 years show higher values due to canopy size and density. GNDVI values were found to decline in trees aged 15–20 years and then increase again in trees over 25 years old.

2.4.2. Selection of predictors

An exploratory analysis was performed to determine the relationships between predictors and yield and their ability to explain variability in yield (Table S2 and Fig. S3). Although varying in magnitude, all the relationships were significant (p-value < 0.05). There was a moderate relationship between current season yield and the yield from the previous 2 years (th_2ys), and a weaker relationship between the current yield and yield from 1 and 3 year(s) ago (th_1ys and th_3ys). There was a weak relationship between yield and tree age and RS data (VIs). However, we noticed that the relationships were slightly stronger when blocks were young and the alternate bearing was not initiated. Moreover, the further the VIs (three years – two years) from current season, the weaker the relationship. In tree crops, the relationship between yield and crop reflectance is often influenced by the tree condition from past harvest season. In other words, there is a lag effect driven by alternate bearing and management such as harvest delays that would subsequently affect flowering, fruit set and yield of the following season. This condition is supported by the highest correlation coefficients ($r > 0.28$) between the VIs at 6P (harvest) of the immediate previous season (1ys) and 1P and 2P of the current season. Particularly, the highest correlated predictor of yield was GNDVI from 1ys at 6P with $R^{\hat{}}2 = 0.33$ (Table S2).

In order to select the best set of predictors, we evaluated multiple sets considering their origin (TS-RS or TS-HY) and the length of the time series (TS) in the context of the six models analyzed. Fig. 5 presents the average of performance metrics corresponding to each predictor set. We conducted One-way ANOVA tests to determine the primary factor influencing prediction accuracy. The results revealed that, in isolation, the model type and set of predictors had a significant effect (p-value $<$ 0.05), on prediction performance but their interaction did not add significant (p-value $>$ 0.05) changes to the prediction accuracies.

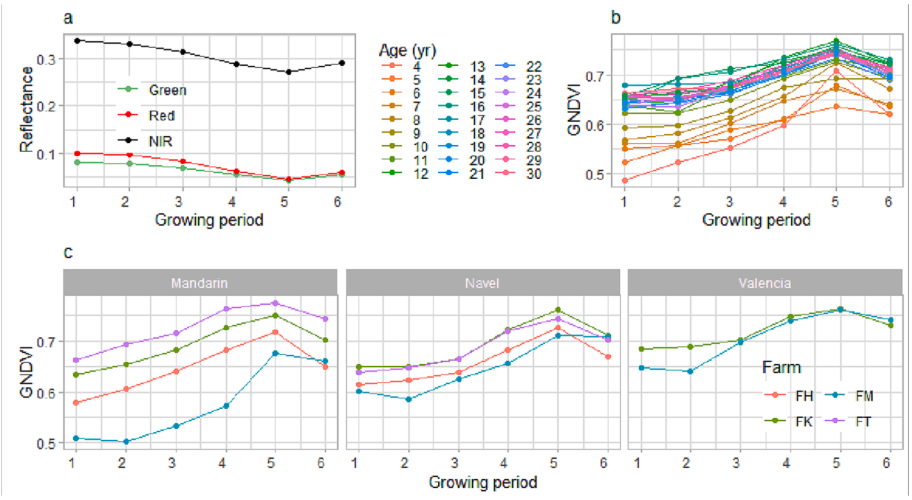

Fig. 4. Average temporal reflectance profiles of the green, red and NIR bands for all citrus types (a) and average GNDVI values according to tree age (b) and farms/locations (c). Lines represent the average values calculated for each period among seasons (from 2007 to 2021). (For interpretation of the references to colour in this figure legend, the reader is referred to the web version of this article.)

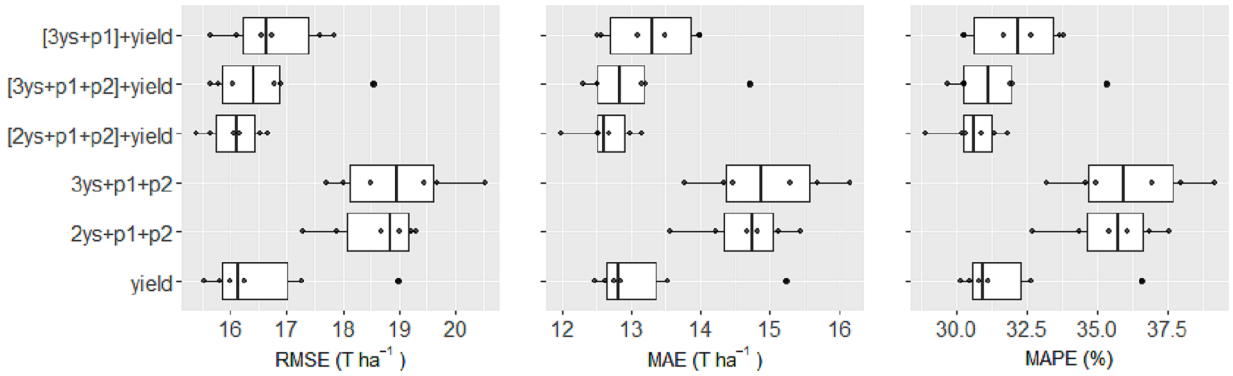

Fig. 5. Average of prediction accuracy parameters among validation seasons. Points represent results per validated model.

Therefore, the selection of set of predictors were based on trends among models. The importance of historical yields in enhancing overall accuracy was evident, while relying solely on TS-RS resulted in a decrease in prediction accuracy (Fig. 5). The minimum differences between parameters were calculated as follows: RMSE of 2 T ha^{-1}, MAE of 1.4 T ha^{-1}, and MAPE of 3.6%. The length of TS-RS did not significantly improve prediction accuracies. Two years of RS data (2y) was better than 3 years (3y) for all prediction parameters. Although not significant, the inclusion of the second period (2P) relative to the current growing season (1p + 2p) slightly improved model performances by overall, reducing the maximums on the prediction accuracies parameters. The combination of both historical yields and RS data (particularly 2ys + 1p + 2p) reduced the maximum of errors regardless the model. Therefore, '[2ys + 1p + 2p] + yield' was selected as the best set of predictors. As 1P and 2P are included as predictors, this implies that forecast can be done by the end of January providing a forecast window between two to nine months prior harvest.

2.4.3. Model performance for yield forecasting at the block level

Overall, svmRadial outperformed with RMSE, MAE and MAPE equivalent to 15.5 T ha^{-1}, 12.1 T ha^{-1} and 29% followed very closely by plsr (15.7 T ha^{-1}, 12.5 T ha^{-1} and 30%). brnn and svmLinear3 performed very similar (16 T ha^{-1}, 12 T ha^{-1} and 30%) whilst xgbLinear (16.7 T ha^{-1}, 13.1 T ha^{-1}, 32%) and pcaNNet (16.7 T ha^{-1}, 13 T ha^{-1}, 31%) yielded the poorest performances among seasons (Fig. 6). The temporal analysis demonstrated the accuracies exhibited significant fluctuations across the validated seasons. The poorest prediction parameters were obtained during 2018 with brnn and xgbLinear (18 T ha^{-1} < RMSE < 19 T ha^{-1}) and the best ones with svmLinear3 and svmRadial during 2019 (RMSE < 13.5 T ha^{-1}). For the majority of the models, the prediction accuracies showed a notable decline in 2020 and 2021, deviating significantly from the average performance. Models had limited power to forecast very high or very low yields (above 100 T ha^{-1} or below 5 T ha^{-1}). Such values were only seen during some of the calibration seasons and blocks (Fig. 2) therefore, the models did not have the sufficient prior learning (temporal nor spatial) to recognize such patters in the future. The fitted lines close to the 1:1 line and the

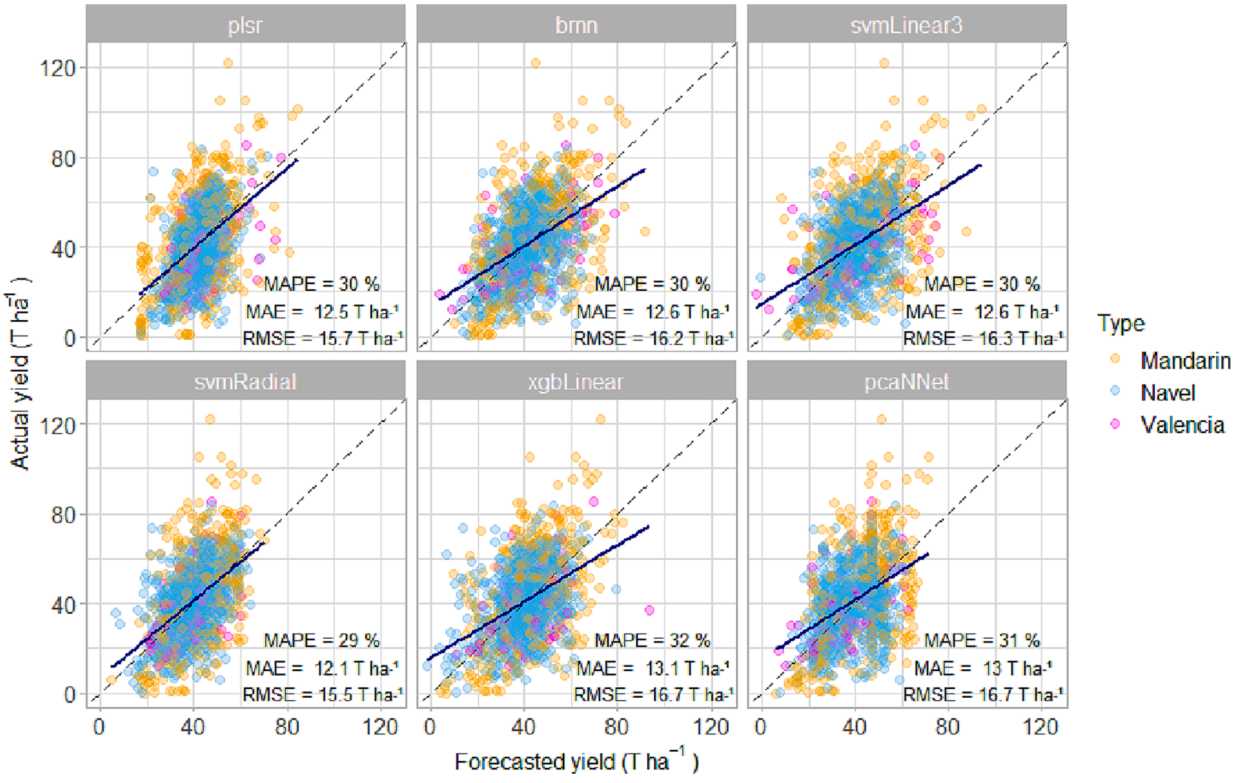

Fig. 6. Comparison between the forecast and actual block-yields over validation season by different models. Each point represent a block from 2017 to 2021.

Table 5
Overall performance of models at different levels of assessment.

Assessment level	Accuracy parameters	Model					
		plsr	brnn	svmLinear3	svmRadial	xgbLinear	pcaNNet
Citrus type	RMSE	16	15	15	13	16	15
	MAE	13	11	11	11	12	12
	MAPE	32%	28%	28%	27%	30%	30%
Location (farm)	RMSE	16	17	17	16	17	17
	MAE	13	13	14	13	13	14
	MAPE	30%	30%	31%	28%	31%	32%
Seasons	RMSE	16	15	17	16	17	17
	MAE	12	12	13	13	13	13
	MAPE	30%	29%	30%	29%	30%	31%

accuracy parameters indicated that the forecasted block-yields with the svmRadial were consistently closer to actual yields than other models (R^2 = 88%). We further assessed the accuracy parameters per citrus type, location (farm) and seasons (Table 5) confirming the svmRadial was, overall, the best performing model across the different levels of analysis. The RMSE at the citrus type level for the svmRadial (13 T ha^{-1}) was the lowest of all models whilst MAPE was the lowest among the different assessment levels (equally with brnn at the season level). Specifically, svmRadial performed well when forecasting yields between 20 T ha^{-1} and 70 T ha^{-1}. However, outside that range, yields were underestimated.

The VImp analysis helps interpret statistical and machine learning models by determining the contribution of each feature to the model's predictions. Although predictions between models were highly correlated (r > 0.63, except for plsr-brnn), the (model-specific) VImp varied considerably per model. For the top performing models (svmRadial and plsr), the yield recorded 2 years before the current season (tha_2ys) was the most significant predictor (Fig. 7). For the svmRadial, the second most important predictors were all the VIs from the first period of the current growing season, followed by the GCVI, GNDVI and NDVI from several periods of the season immediate before (except 5P). Mostly, all the periods of the immediate before season were relatively important. Plsr is also integrating VIs but with limited relative importance as the top three predictors are all historical yields.

According to the calculated MBE (data not presented), the models underestimated yields in three seasons and overpredicted in two seasons. The largest discrepancies were observed in the 2020, with an average MBE of −6.7 T ha^{-1}, followed by the 2021 season, with an average MBE of + 5.6 T ha^{-1}. The 2020 season stood out from the average (Fig. 2) as Mandarin blocks produced exceptionally high yields, leading to underestimation by all models. On the other hand, the 2021 season was relatively more average, resulting in overestimation. This finding highlights the significant influence of the yields from the immediate previous season (tha_1yr) on the current season, suggesting the depletion of the source- sink of tree resources. plsr better captured this relationship compared to svmRadial. In plsr, 'tha_1yr' ranked among the top three most important variables, whereas in svmRadial, it was the 20th most important variable. However, the heavy reliance of plsr on historical yields may limit the availability of data for a particular block. Therefore, a shorter historical yield requirement is preferable to mitigate this issue.

Although prediction accuracy parameters were similar, the svmRadial model was chosen as the best model for forecasting block-yields as it shown greater stability across validation seasons, citrus type, and locations (Fig. 6 and Table 5). Fig. 8 shows the spatial distribution of actual and forecast yields for 2021 season and the quantified errors highlighting blocks with underestimated/overestimated yields.

2.4.4. *Estimation of seasonal total production*

Assessing the temporal variability at different levels of aggregation provides valuable insights into the accuracy of our chosen model (svmRadial) for forecasting production trends. This analysis is particularly crucial for end users, as it enables them to make informed decisions to ensure market security, pricing stability, and effective allocation of resources at both industry and farm levels. Moreover, understanding the spatial distribution of production per block offers a powerful tool for planning farm management operations, including fertilization and irrigation scheduling.

Using the svmRadial model, we calculated the total production (in tons, T) for each block by multiplying the planted area (ha) with the block-yield (T). We then aggregated the values per citrus type (refer to Fig. 9). Overall, our model successfully captured the temporal variability in production for Valencia and Navel, with the exception of 2021. The average production estimate errors at the citrus type level were 15% for Mandarin and 11% for Navels and Valencia. The highest errors occurred in Mandarin and Navel blocks during 2020 and 2021. As previously

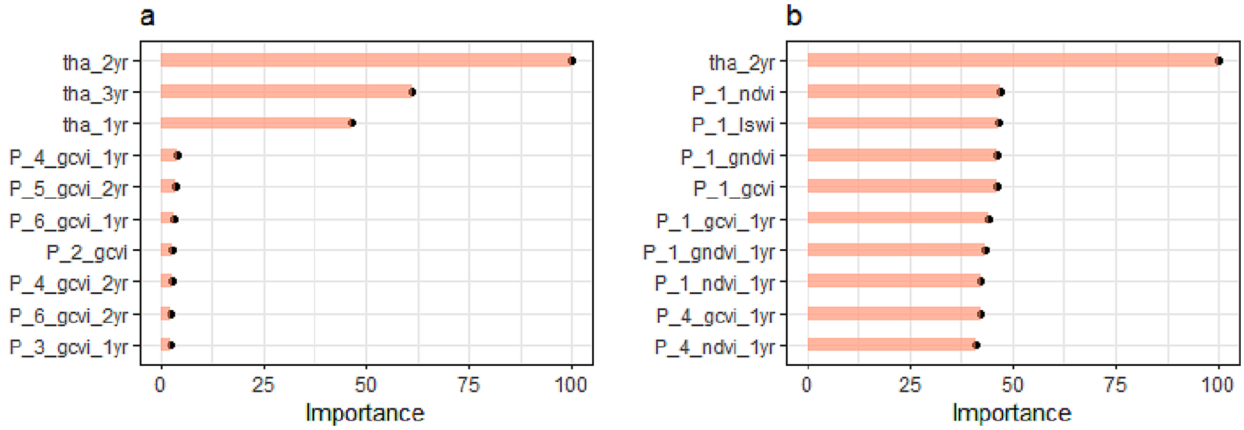

Fig. 7. Model-specific variable of importance for block-level yield forecasting: plsr (a) and svmRadial (b), showing the top 10 most important features.

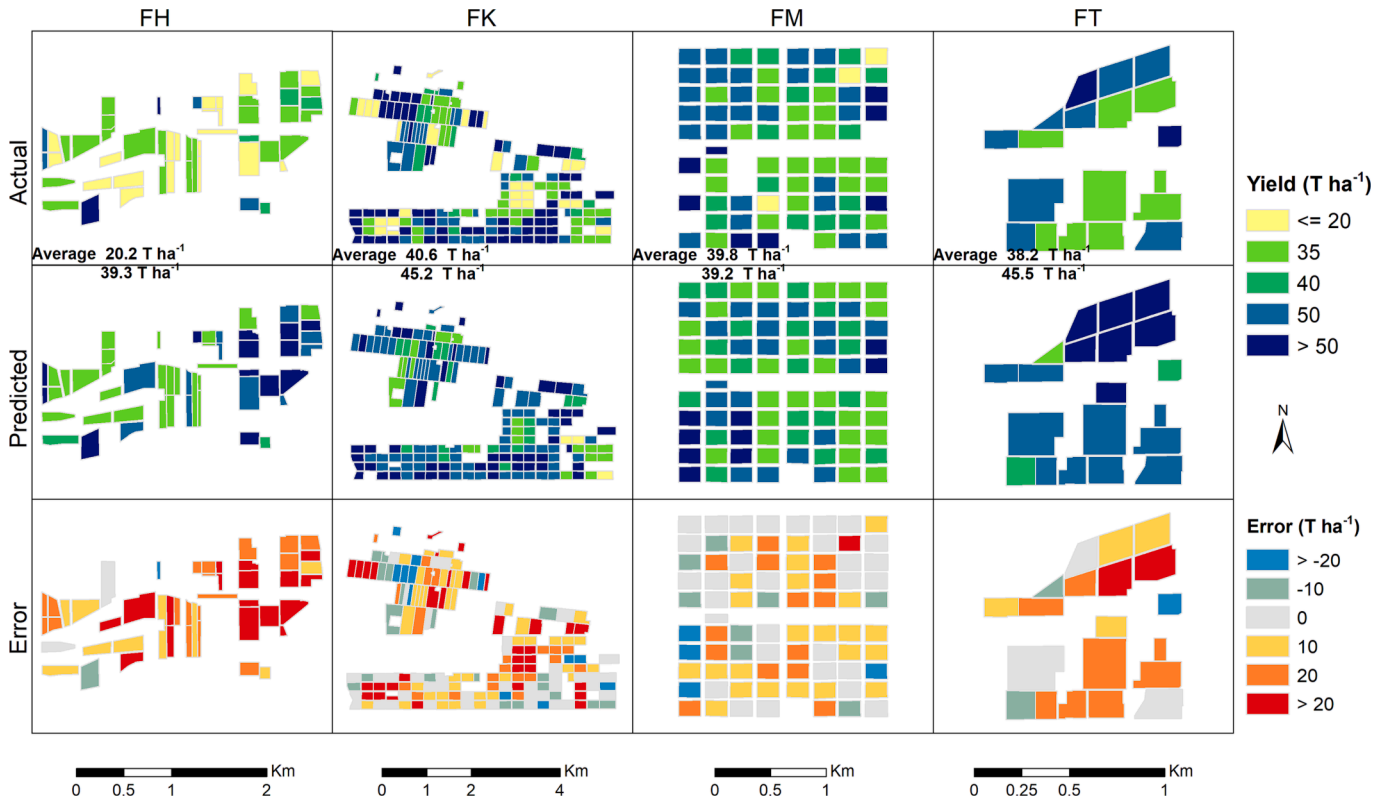

Fig. 8. Spatial comparison of forecasted and actual block-yields for 2021 season and quantified error (T ha^{-1}).

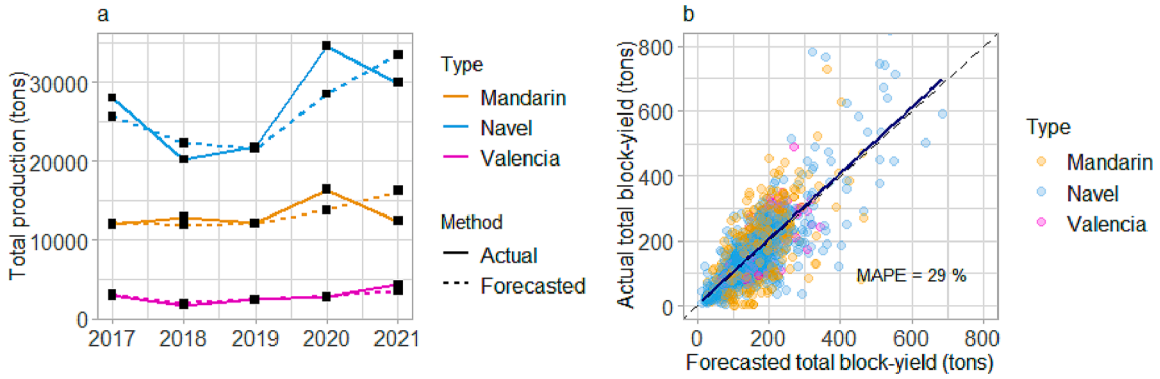

Fig. 9. Comparisons of actual and forecasted total production per citrus type (a) and total block-level yield (b) with svmRadial during 2017–2021. Each point represents a block from 2017 to 2021.

explained, these two seasons, especially 2020, witnessed exceptionally high yields, and our models did not possess prior knowledge to account for such scenarios, resulting in poorer performance.

3. Discussion

3.1. Reflectance profiles of citrus orchards

The bimonthly RS aggregation aligned with key developmental growth stages. The reflectance profiles of the citrus crops are similar to avocado crops as reported in Rahman et al. (2022) where the maximums VIs values were obtained during maturation whilst the minimum values were acquired during flowering. At flowering the chlorophyll content is relatively lower in comparison to other growth stages (Mustafa et al., 2005). A constant increment of the VIs was also obtained during the vegetative growth equivalent to 3P-4P in this study. Although in Rahman et al. (2022) there was no analysis according to tree age, the variability per locations (farms) was also proved. Identifying these growth profiles alone offers significant benefit to growers as it can be used to benchmark 'normal' seasonal and locational performance. Any significant deviation or delays in the temporal pattern during a subsequent growing year can indicate the incidence of tree stress (e.g. pest, disease, climatic) and as such can serve as an early warning system for grower intervention. On a macro scale large variations in all crops can indicate changing growth patterns potentially associated with a changing climate.

3.2. Set of predictors for block-yield forecasting

Our forecasting models leveraged freely available remote sensing data and historical block-yield records to predict yields. The selection of predictors and model type had a significant impact on prediction

accuracy. Including the previous two years' yields as predictors proved essential for capturing temporal production variability caused by biennial bearing. Our analysis demonstrated strong correlations between the current yield and yields from two years prior, supporting the presence of biennial bearing at the block level. Removing these parameters led to decreased accuracy, as the yields from two years prior were the most important variable for accurate yield forecasting. Additionally, the correlations between the VIs of the first two periods of the current season (1P and 2P) and yield aligned with fruit growth stages, emphasizing the relevance of crop load and fruit set adjustments (Khurshid and Braysher, 2009). Mustafa et al. (2005) highlighted the suitability of remote sensing techniques during the fruit setting stage for monitoring citrus crops. Consequently, both historical yields and remote sensing-derived vegetation indices offered valuable insights into the intricate interactions at the tree and block level.

3.3. Model performance and block-yield forecasting: Implications

Compared to annual crops like wheat, maize, and rice, there is limited research on yield forecasting for tree crops at the block-level (Benos et al., 2021; Schauberger et al., 2020). This study addresses this gap by compiling one of the largest citrus datasets in the literature, consisting of over 3500 yield records spanning 14 years of historical production. The dataset encompasses diverse citrus varieties, tree ages, management practices, and locations, the strengthening the transferability of the models.

In commercial practice, yield forecasts for citrus are typically performed three times during the growing season: after harvest, after fruit set, and closer to harvest. Among these, the estimate after fruit set is particularly significant as it provides valuable insights for market access and adjustment of management practices (Anderson et al., 2021b; Ye et al., 2007), and it is the focus of this study. The current approach involves manual counting of fruit on a sample of trees, resulting in reported average accuracy errors ranging from 8% to 57% (average of 27%) (Anderson et al., 2021a). This labor-intensive method requires visits to each block within a farm and relies on the number of selected trees, consuming significant human and logistical resources. In contrast, our proposed method not only achieves acceptable accuracies but also eliminates the need for labor-intensive sampling during the growing season, providing a cost-effective and viable alternative for industry adoption. Importantly, our forecasting model utilizes data up to the end of fruit set (2P), enabling yield forecasts to be provided two to nine months prior to harvest.

The assessment of accuracy parameters was used to determine the best model for citrus block-yield forecasting. svmRadial outperformed other algorithms, with results very similar to plsr. However, the (relative) variable of importance (VImp) varied per model indicating that each model is capturing unique information or patterns that are relevant for predicting citrus block-yield and so the models performed best on different subsets of the data. Understanding how the model made its predictions supported model selection and built trust in the decision. svmRadial was less dependent on historical yields and utilized the information provided by VIs on crop condition. Therefore, in the absence of historical yields, svmRadial is expected to perform within acceptable accuracy ranges. The choice of svmRadial as the best model was influenced by its interpretability, understanding of prediction mechanisms, and specific requirements of the end-users. Additionally, svmRadial demonstrated the ability to forecast production trends which can provide insights into alternate bearing aiding more informed decisions (Zhang et al., 2019).

While the high performance of svmRadial indicated a nonlinear relationship between predictors and yield, it is important to note that the choice of the best model appears to depend on the specific cropping system being evaluated. Brinkhoff and Robson (2021) found that the linear model using ridge regularized regression consistently performed better in forecasting macadamia yields compared to other algorithms, including svmRadial. Similarly, Zhang et al. (2019) tested random forest and stochastic gradient boosting (SGB) and found that SGB outperformed when forecasting almond block yields. In contrast, the gradient boosting algorithm (xgbLinear) had poor performance in this study. These outcomes highlight the importance of considering different machine learning approaches and comparing their performance when conducting similar analyses in other crops.

The primary objective of this research was to develop a robust yield forecasting model for citrus at the block level, utilizing a wide range of variables, including canopy reflectance properties and historical production data. By examining multiple blocks, seasons, locations, and varieties, the study aimed to identify the most reliable approach or model for predicting yield, independent of the various influencing factors (abiotic and biotic) that affect production. The obtained results are encouraging, demonstrating a more scalable and potentially automated methodology that does not necessitate a comprehensive understanding and incorporation of all potential constraints.

Although this methodology may not provide detailed insights into within-block constraints or guide precision agriculture practices, it offers a valuable foundation for yield prediction across a broader context. To address specific within-orchard constraints, further research and a deeper understanding would be required. However, it is crucial to note that such specific applications were not the primary focus of this study.

3.3.1. Model assessment

Comparisons with other studies are challenging due to variations in dataset characteristics, hence RMSE values are not comparable (Schauberger et al., 2020). According to Basso and Liu (2019), most of the studies using RS models for forecasting yield in the mid-season reported R^2 values (between forecasted and actual yields) of 0.6–0.8. Our study fits well with an R^2 equal to 0.88 across validation seasons. Brinkhoff and Robson (2021) reported MAPE equal to 22.9%. Our MAPE value across validation seasons was 6.2% higher. Given the substantial variability observed in our dataset (standard deviation = 17.8 T ha^{-1} or 48.8%), the prediction accuracies achieved can be deemed acceptable. Studies in citrus have focused on few small blocks with one particular variety usually based on fruit detection and counting with data calibrated from the same growing season (Dorj et al., 2017; Rosell et al., 2009; Rosell Polo et al., 2009). Although more accurate results were reported ($R^2 > 0.9$), the utility of such approaches for large areas with short returning time is strongly limited and the need to the provision of early yield estimates is not met. Alternative approaches using machine-vision systems and UAVs have been explored but face limitations due to small fruitlet size and occlusions caused by other fruit, branches, or leaves (Anderson et al., 2021b; Lee et al., 2010). These limitations produced errors exceeding 53% when estimating fruit yield around 90 days before harvest (Anderson et al., 2021a). With differences between actual and forecasted total production varying from 15% (Mandarin) to 11% (Navel and Valencia), our approach is an essential improvement for forecasting block-yields early in the season (just after the physiological drop) regardless the citrus varieties and location.

3.3.2. Limitations of early yield forecasting

The biophysical and biochemical traits of fruit trees regulate their structural, physiological, and phenological properties at the leaf, canopy, and block level (Ali and Imran 2021). In this study, we forecast yield taking in consideration historical production and reflectance-based information which is highly related to canopy structure and health (Mulla, 2013). Hence, some of the weakness of yield forecasting accuracies can be related to external factors such as abiotic and biotic stressors, harvest operations, management decisions, and measurement errors rather than model performance (Anderson et al., 2021b; Lobell, 2013; Schauberger et al., 2020). For example, in this study, there was a large hailstorm at the end of January 2021 affecting most of the blocks of

the FH farm. As the impact of the hailstorm was severe so was the pruning (after forecast was performed) reducing significantly the actual yield over those blocks and therefore, large forecasting errors were obtained. That said, the reported errors may reflect the gap between the actual and potential yield (yield gap). Quantifying this yield gap is crucial for informing policies and decision-making to minimize environmental impacts and improve production (Van Wart et al., 2013).

3.3.3. Scalability of citrus block-yield forecasting

In contrast to annual crops, tree crops lack rotation and can be considered "fixed" as planted blocks can remain productive for over 30 years. While this study relied on crop boundaries provided by growers, the methodology employed is adaptable to mapping products like The Australian Tree Crop Map Dashboard (ATCM) developed by McKechnie and Shephard (2021), which offers block boundaries at a national scale. Although the highest accuracy is achieved when models have access to historical yield data, this study also evaluated the impact of using only time-series remote sensing (TS-RS) data on model performance. The results showed that the prediction accuracies obtained solely from TS-RS data were within acceptable levels (Fig. S4). This finding suggests that our method can be successfully implemented on a national scale, leveraging the global availability of predictor datasets such as Landsat.

4. Conclusion

Our study contributes to the limited research on block-level yield forecasting for tree crops, showcasing the potential of remote sensing data and historical yield records for accurate predictions. The methodology presented here offers a cost-effective alternative to labor-intensive sampling during the growing season, making it suitable for wider adoption in the citrus industry. We calibrated and validated various statistical and machine learning algorithms, ultimately selecting the svmRadial model for its superior prediction accuracy. This model accurately forecasted block-level yields across multiple farms, varieties, and seasons from 2017 to 2021, with an RMSE of 15.5 T ha^{-1}, R2 of 0.88, MAE of 12.1 T ha^{-1}, and MAPE of 29%. Although the model faced limitations in forecasting outliers, it effectively captured the temporal variability of production at different levels of aggregation (citrus type). Furthermore, our proposed method can be implemented on a national scale due to its utilization of freely available Landsat imagery.

5. Data statement

Scripts and codes to access Landsat or any other image collection are freely available in https://developers.google.com/earth-engine/tutorials/community/explore.

The code for modeling will be available from the corresponding author upon request.

The block data have been collated under the Rural R&D for Profit program founded by the Australian Government Department of Agriculture and Water Resources. There are restrictions to the usability of the yield data, which were used under special permission and are not publicly available. However, it can be available from the corresponding author upon reasonable request and prior approval. The data are not publicly available for legal and/or ethical reasons.

CRediT authorship contribution statement

Luz Angelica Suarez: Conceptualization, Data curation, Methodology, Validation, Formal analysis, Investigation, Writing – original draft, Writing – review & editing, Visualization, Project administration. **Andrew Robson:** Writing – review & editing, Supervision, Project administration, Funding acquisition. **James Brinkhoff:** Conceptualization, Methodology, Writing – review & editing.

Declaration of Competing Interest

The authors declare that they have no known competing financial interests or personal relationships that could have appeared to influence the work reported in this paper.

Data availability

The historical production have been collated under the Rural R&D for Profit program founded by the Australian Government Department of Agriculture and Water Resources. There are restrictions to the usability of the yield data, which were used under special permission and are not publicly available. However, it can be available from the corresponding author upon reasonable request and prior approval. The data are not publicly available for legal and/or ethical reasons. The code for modeling will be available from the corresponding author upon request. Scripts and codes to access Landsat or any other image collection are freely available in https://developers.google.com/earth-engine/tutorials/community/explore

Acknowledgment

This project was founded by the Australian Government Department of Agriculture and Water Resources as part of its Rural R&D for Profit program – and UNE as the co-investor for ST19008 and ST19015. The authors are grateful for the support of the Australian citrus industry and the participant growers for providing production data.

Appendix A. Supplementary data

Supplementary data to this article can be found online at https://doi.org/10.1016/j.jag.2023.103434.

References

Ali, A., Imran, M., 2021. Remotely sensed real-time quantification of biophysical and biochemical traits of Citrus (Citrus sinensis L.) fruit orchards – A review. ScientiaHorticulturae 282, 110024.
Anderson, N.T., Walsh, K.B., Koirala, A., Wang, Z., Amaral, M.H., Dickinson, G.R., Sinha, P., Robson, A.J., 2021a. Estimation of Fruit Load in Australian Mango Orchards Using Machine Vision. Agronomy 11, 1711.
Anderson, N.T., Walsh, K.B., Wulfsohn, D., 2021b. Technologies for Forecasting Tree Fruit Load and Harvest Timing—From Ground, Sky and Time. Agronomy 11, 1409.
Basso, B., Liu, L., 2019. Chapter Four - Seasonal crop yield forecast: Methods, applications, and accuracies. In: Sparks, D.L. (Ed.), Advances in Agronomy. Academic Press, pp. 201–255.
Benos, L., Tagarakis, A.C., Dolias, G., Berruto, R., Kateris, D., Bochtis, D., 2021. Machine Learning in Agriculture: A Comprehensive Updated Review. Sensors 21, 3758.
Bevington, K., HArdy, S., Melville, P., Thiel, K., Fullelove, G., Morrish, P.M., 2003. Fruit Size Management Guide - Part 1.
Brinkhoff, J., Robson, A.J., 2021. Block-level macadamia yield forecasting using spatio-temporal datasets. Agric. For. Meteorol. 303, 108369.
Bureau of Meteorology, 2023. Climate classification maps, Köppen major classes.
Chandrasekar, K., Sesha Sai, M.V.R., Roy, P.S., Dwevedi, R.S., 2010. Land Surface Water Index (LSWI) response to rainfall and NDVI using the MODIS Vegetation Index product. Int. J. Remote Sens. 31 (15), 3987–4005.
de Myttenaere, A., Golden, B., Le Grand, B., Rossi, F., 2016. Mean Absolute Percentage Error for regression models. Neurocomputing 192, 38–48.
Dorj, U.-O., Lee, M., Yun, S.-S., 2017. An yield estimation in citrus orchards via fruit detection and counting using image processing. Comput. Electron. Agric. 140, 103–112.
Gitelson, A.A., 2011. Remote sensing estimation of crop biophysical characteristics at various scales, Hyperspectral Remote Sensing of Vegetation. CRC Press 329–358.
Gitelson, A.A., Gritz †, Y., Merzlyak, M.N., 2003. Relationships between leaf chlorophyll content and spectral reflectance and algorithms for non-destructive chlorophyll assessment in higher plant leaves. J. Plant Physiol. 160 (3), 271–282.
Gomez, D., Salvador, Sanz-Justo, J., Casanova, J.-L., 2019. Potato Yield Prediction Using Machine Learning Techniques and Sentinel 2 Data. Remote Sens. (Basel) 11, 1745.
Gorelick, N., Hancher, M., Dixon, M., Ilyushchenko, S., Thau, D., Moore, R., 2017. Google Earth Engine: Planetary-scale geospatial analysis for everyone. Remote Sens. Environ. 202, 18–27.
Greenwell, B.M., Boehmke, B.C., McCarthy, A.J., 2018. A simple and effective model-based variable importance measure. arXiv preprint arXiv:1805.04755.

Iglesias, D.J., Cercós, M., Colmenero-Flores, J.M., Naranjo, M.A., Ríos, G., Carrera, E., Ruiz-Rivero, O., Lliso, I., Morillon, R., Tadeo, F.R., Talon, M., 2007. Physiology of citrus fruiting. Braz. J. Plant Physiol. 19 (4), 333–362.
Isagi, Y., Sugimura, K., Sumida, A., Ito, H., 1997. How Does Masting Happen and Synchronize? J. Theor. Biol. 187 (2), 231–239.
Kato, T., 2016. Chapter 4 - Prediction of photovoltaic power generation output and network operation. In: Funabashi, T. (Ed.), integration of Distributed Energy Resources in Power Systems. Academic Press, pp. 77–108.
Khurshid, T., Braysher, B., 2009. Early Fruit Size Prediction Model Using Cubic Smoothing Splines for 'Washington Navel' (Citrus Sinensis L. Osbeck) Oranges in Australia. International Journal of Fruit Science 9 (4), 394–408.
Kim, N., Ha, K.-J., Park, N.-W., Cho, J., Hong, S., Lee, Y.-W., 2019. A Comparison Between Major Artificial Intelligence Models for Crop Yield Prediction: Case Study of the Midwestern United States, 2006–2015. ISPRS Int. J. Geo Inf. 8, 240.
Koirala, A., Walsh, K.B., Wang, Z., McCarthy, C., 2019. Deep learning for real-time fruit detection and orchard fruit load estimation: benchmarking of 'MangoYOLO'. Precis. Agric. 20 (6), 1107–1135.
Konduri, V.S., Vandal, T.J., Ganguly, S., Ganguly, A.R., 2020. Data Science for Weather Impacts on Crop Yield. Frontiers in Sustainable Food Systems 4.
Kuhn, M., 2008. Building predictive models in R using the Caret package. J. Stat. Softw. 28.
Kuhn, M., Johnson, K., 2016. Applied Predictive Modeling. Springer.
Lee, W.S., Alchanatis, V., Yang, C., Hirafuji, M., Moshou, D., Li, C., 2010. Sensing technologies for precision specialty crop production. Comput. Electron. Agric. 74 (1), 2–33.
Lee, D., Davenport, F., Shukla, S., Husak, G., Funk, C., Harrison, L., McNally, A., Rowland, J., Budde, M., Verdin, J., 2022. Maize yield forecasts for Sub-Saharan Africa using Earth Observation data and machine learning. Glob. Food Sec. 33, 100643.
Leukel, J., Zimpel, T., Stumpe, C., 2023. Machine learning technology for early prediction of grain yield at the field scale: A systematic review. Comput. Electron. Agric. 207, 107721.
Lobell, D.B., 2013. The use of satellite data for crop yield gap analysis. Field Crop Res 143, 56–64.
Luo, Y., Zhang, Z., Cao, J., Zhang, L., Zhang, J., Han, J., Zhuang, H., Cheng, F., Tao, F., 2022. Accurately mapping global wheat production system using deep learning algorithms. International Journal of Applied Earth Observation and Geoinformation 110, 102823.
McKechnie, J., Shephard, C., 2021. Mapping Horticulture Tree Crops in Australia.
Mkhabela, M.S., Bullock, P., Raj, S., Wang, S., Yang, Y., 2011. Crop yield forecasting on the Canadian Prairies using MODIS NDVI data. Agric. For. Meteorol. 151 (3), 385–393.
Mulla, D.J., 2013. Twenty five years of remote sensing in precision agriculture: Key advances and remaining knowledge gaps. Biosyst. Eng. 114 (4), 358–371.
Mustafa, S., Sonmez, N.K., Karaca, M., 2005. Relationship between chlorophyll content and canopy reflectance in Washington navel orange trees (Citrus sinensis (L.) Osbeck). Pak. J. Bot. 37, 1093–1102.
Notton, G., Voyant, C., 2018. Chapter 3 - Forecasting of Intermittent Solar Energy Resource. In: Yahyaoui, I. (Ed.), Advances in Renewable Energies and Power Technologies. Elsevier, pp. 77–114.
Perez, R., Cebecauer, T., Šúri, M., 2013. Chapter 2 - Semi-Empirical Satellite Models. In: Kleissl, J. (Ed.), Solar Energy Forecasting and Resource Assessment. Academic Press, Boston, pp. 21–48.
R Core Team, 2014. R: A language and environment for statistical computing. R Foundation for Statistical Computing, Viena, Austria.
Rahman, M., Robson, A., Bristow, M., 2018. Exploring the Potential of High Resolution WorldView-3 Imagery for Estimating Yield of Mango. Remote Sens. (Basel) 10, 1866.
Rahman, M., Robson, A., Brinkhoff, J., 2022. Potential of Time-Series Sentinel 2 Data for Monitoring Avocado Crop Phenology. Remote Sens. (Basel) 14, 5942.
Robson, A., Rahman, M., Muir, J., 2017a. Using Worldview Satellite Imagery to Map Yield in Avocado (Persea americana): A Case Study in Bundaberg. Australia. Remote Sensing 9, 1223.
Robson, A., Rahman, M.M., Muir, J., Saint, A., Simpson, C., Searle, C., 2017b. Evaluating satellite remote sensing as a method for measuring yield variability in Avocado and Macadamia tree crops. In: Taylor, J.A. (Ed.), 11th European Conference on Precision Agriculture (ECPA 2017). Advances in Animal Biosciences, Cambridge University Press, pp. 498–504.
Rosell, J.R., Llorens, J., Sanz, R., Arnó, J., Ribes-Dasi, M., Masip, J., Escolà, A., Camp, F., Solanelles, F., Gràcia, F., Gil, E., Val, L., Planas, S., Palacín, J., 2009. Obtaining the three-dimensional structure of tree orchards from remote 2D terrestrial LIDAR scanning. Agric. For. Meteorol. 149 (9), 1505–1515.
Rosell Polo, J.R., Sanz, R., Llorens, J., Arnó, J., Escolà, A., Ribes-Dasi, M., Masip, J., Camp, F., Gràcia, F., Solanelles, F., Pallejà, T., Val, L., Planas, S., Gil, E., Palacín, J., 2009. A tractor-mounted scanning LIDAR for the non-destructive measurement of vegetative volume and surface area of tree-row plantations: A comparison with conventional destructive measurements. Biosyst. Eng. 102 (2), 128–134.
Rosipal, R., Trejo, L.J., 2002. Kernel partial least squares regression in reproducing kernel hilbert space. J. Mach. Learn. Res. 2, 97–123.
Sakai, K., Noguchi, Y., Asada, S.-I., 2008. Detecting chaos in a citrus orchard: Reconstruction of nonlinear dynamics from very short ecological time series. Chaos Solitons Fractals 38 (5), 1274–1282.
Schauberger, B., Jägermeyr, J., Gornott, C., 2020. A systematic review of local to regional yield forecasting approaches and frequently used data resources. Eur. J. Agron. 120, 126153.
Scholbeck, C.A., Molnar, C., Heumann, C., Bischl, B., Casalicchio, G., 2020. Sampling, intervention, prediction, aggregation: a generalized framework for model-agnostic interpretations, Machine Learning and Knowledge Discovery in Databases: International Workshops of ECML PKDD 2019, Würzburg, Germany, September 16–20, 2019, Proceedings, Part I. Springer, pp. 205-216.
Sola-Guirado, R.R., Castillo-Ruiz, F.J., Jiménez-Jiménez, F., Blanco-Roldan, G.L., Castro-Garcia, S., Gil-Ribes, J.A., 2017. Olive Actual "on Year" Yield Forecast Tool Based on the Tree Canopy Geometry Using UAS Imagery. Sensors (Basel, Switzerland) 17, 1743.
Somers, B., Delalieux, S., Verstraeten, W.W., Eynde, A.V., Barry, G.H., Coppin, P., 2010. The Contribution of the Fruit Component to the Hyperspectral Citrus Canopy Signal. Photogramm. Eng. Remote Sens. 76 (1), 37–47.
Stephenson, R.A., Cull, B.W., Stock, J., 1986. Vegetative flushing patterns of macadamia trees in south east Queensland. ScientiaHorticulturae 30 (1-2), 53–62.
Stuckens, J., Dzikiti, S., Verstraeten, W.W., Verreynne, S., Swennen, R., Coppin, P., 2011. Physiological interpretation of a hyperspectral time series in a citrus orchard. Agric. For. Meteorol. 151 (7), 1002–1015.
Tucker, C.J., 1979. Red and photographic infrared linear combinations for monitoring vegetation. Remote Sens. Environ. 8 (2), 127–150.
Van Wart, J., Kersebaum, K.C., Peng, S., Milner, M., Cassman, K.G., 2013. Estimating crop yield potential at regional to national scales. Field Crop Res 143, 34–43.
Ye, X., Sakai, K., Manago, M., Asada, S.-I., Sasao, A., 2007. Prediction of citrus yield from airborne hyperspectral imagery. Precis. Agric. 8 (3), 111–125.
Ye, X., Sakai, K., Asada, S.I., Sasao, A., 2008. Inter-Relationships Between Canopy Features and Fruit Yield in Citrus as Detected by Airborne Multispectral Imagery. Trans. ASABE 51, 739–751.
Zhang, Z., Jin, Y., Chen, B., Brown, P., 2019. California Almond Yield Prediction at the Orchard Level With a Machine Learning Approach. Frontiers. Plant Sci. 10.